Microseismicity Induced by Deep Wastewater Injection in Southern Trumbull County, Ohio

by Robert J. Skoumal, Michael R. Brudzinski, and Brian S. Currie

Online Material: Description and figure representing the stratigraphy and construction of the two wastewater disposal wells.

INTRODUCTION

As oil and gas well completions utilizing multistage hydraulic fracturing have become more commonplace, the potential for seismicity induced by the deep disposal of frac-related wastewater and the hydraulic fracturing process itself has become an increasingly important issue (e.g., National Academy of Science [NAS], 2012). Although it is rare for a wastewater disposal well to induce felt seismicity, there have been several cases over the past half century that identify strong relationships between injected fluids and seismicity (e.g., Healy *et al.*, 1968; Nicholson and Wesson, 1990; McGarr *et al.*, 2002; Evans *et al.*, 2012). Following the 2011 Youngstown earthquake sequence (YES) near a wastewater disposal well in northeastern Ohio (Fig. 1), which included hundreds of earthquakes up to an **M** 4.0 (Ohio Department of Natural Resources [ODNR], 2012; Kim, 2013; Skoumal, Brudzinski, Currie, *et al.*, 2014), there has been a heightened concern over seismicity related to energy technologies in Ohio. The ODNR is actively setting new regulations to deal with induced seismicity (ODNR, 2014), which could serve as a blueprint for other states. Seismic monitors are to be installed near certain injection wells before commercial injection begins and will remain there for 12 months afterward. A number of regional long-standing backbone seismic stations have been operating for over a decade, and studies of the YES significantly benefited from early adoption of EarthScope Transportable Array (TA) stations in western Pennsylvania in late 2010.

The first earthquake detected by the ODNR and the U.S. Geological Survey in the Trumbull County sequence was an M_L 2.1 earthquake on 31 August 2014 at 21:34 UTC (5:34 p.m. local), with only a single felt report. Epicentral locations placed it within 1 km of the American Water Management Services (AWMS) Weathersfield injection well site, near Warren, Ohio (Fig. 1). There is a shallower well at this site (AWMS-1) that injects into the Silurian interval, and a deeper well (AWMS-2) that injects into the Ordovician–Cambrian interval about 15 m above the Precambrian basement (Ⓔ a description and Fig. S1 representing the stratigraphy and well construction are included in the electronic supplement to this article). AWMS-2 was approved on 4 March 2014 to inject at pressures up to 11.6 MPa (1680 psi). AWMS-1 was approved on 4 March 2014 at 7.1 MPa (1025 psi), which was later raised to 8.3 MPa (1200 psi) on 11 July 2014. As of 31 August 2014, >9160 and $>174,000$ barrels of wastewater were injected into AWMS-1 and AWMS-2, respectively.

The ODNR issued a chief's order on 3 September 2014 suspending operations at both wells. After analyzing data during the investigation, the ODNR spokeswoman Bethany McCorkle said the agency found the shallower of the two wells was not related to the seismic event. On 18 September 2014, the company was allowed to resume injection operations at the shallow well (AWMS-1), while the investigation continued on the deeper well (AWMS-2). In this study, we use multistation waveform template matching as an earthquake fingerprint scanning technique to investigate the potential relationship between the earthquake and the injection operations.

DATA AND ANALYSIS

Our analysis followed the approach of Skoumal, Brudzinski, Currie, *et al.* (2014) that was optimized for the 2011–2014 YES that occurred ~11.5 km away from the Trumbull sequence. Regional seismic data were obtained using Incorporated Research Institutions for Seismology (IRIS) webservices (http://service.iris.edu; last accessed February 2015) and mainly consisted of high-quality broadband EarthScope TA stations recording at 40 samples/s (Fig. 1). The ODNR also sent a hard disk with seismic recordings from 1 July–30 September 2014 from a local four-station network consisting of three-component short-period instruments recording at 200 samples/s (Fig. 1).

Templates using regional data were created for the M_L 2.1 and 1.5 events using the same parameters (e.g., template length, sampling interval) as in previous work (e.g., Skoumal, Brudzinski, Currie, *et al.*, 2014). The preliminary analysis used data from M54A, N54A, and O56A (begun in 6 November 2010), as well as closer stations M53A and N53A (begun 14 January 2013) and operated until 14 January 2015. Local network data were interpolated to a common sampling interval of 100 samples/s and then band-pass filtered between 1 and 45 Hz. Templates of 6 s length starting 1 s before the *P* wave were created from the M_L 2.1 and 1.5 earthquakes. Considering the higher resolution

 doi: 10.1785/0220150055

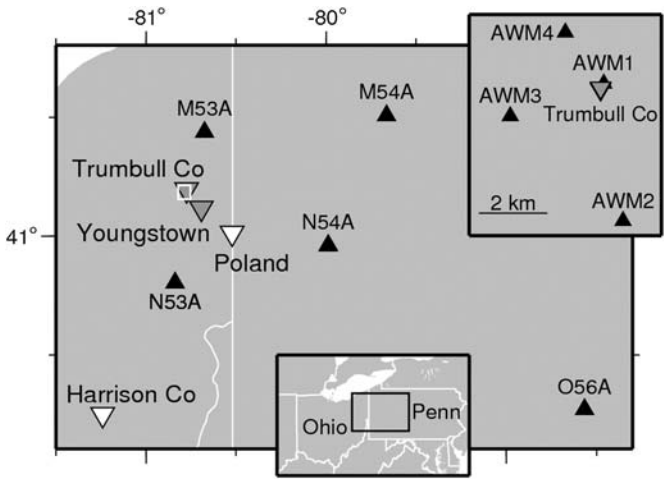

▲ **Figure 1.** Location of the study region (box in the lower inset), with enlarged views showing seismic stations (black triangles) and cases of seismicity that are potentially induced by injection wells (gray) or hydraulic fracturing (white). The white box in the central map is the location of the upper right inset that shows the local seismic network deployed by Ohio Department of Natural Resources (ODNR).

of the local data, an empirical subspace detector was employed to expand the set of matches (Barrett and Beroza, 2014). With this approach, the stack of events and the time derivative of the stack are close approximations of the first two singular vectors. So, for each of the two template match results (M_L 2.1 and 1.5), we created an additional template from the stack of those matches and a template from the time derivative of the stack. We also found that using the derivative of the original template waveforms detected some additional legitimate events. The matches from all eight templates were then combined into our final set of events.

Multistation template matching followed the approach of previous work (e.g., Skoumal, Brudzinski, Currie, *et al.*, 2014). Events were detected if the network normalized cross-correlation coefficient (NNCCC) exceeded an initial threshold of 12 times the median absolute deviation (MAD) of the daily NNCCC for regional data and 8 × MAD for the local data. These thresholds were determined after inspecting the quality of the matched waveforms and the temporal patterns of the matches. Detections were considered legitimate earthquakes if they had a signal-to-noise ratio > 2 and visually resembled the template waveform at the quietest station.

Because of the proximity of this sequence to the YES, we used velocity model B from Kim (2013), which was developed using sonic logs for location analysis with local data. A different velocity model for the YES was previously used because we were using regional data to locate those events (Skoumal, Brudzinski, Currie, *et al.*, 2014), but we found the Kim (2013) model B produced lower residuals in this case, likely due to the availability of local data.

Lag times and correlation coefficients were generated between the template and each matched event to determine wave arrival times and weights for all matched events, which were used with *elocate* (Herrmann, 2004) and the velocity model to determine an initial set of catalog locations. A full set of lag and correlation matrices between all events for all channels were then used in a *hypoDD* double-difference algorithm to determine the relative locations of the events (Waldhauser and Ellsworth, 2000; Waldhauser, 2001). The median relative locations errors that we found based on bootstrapping estimation were 60 m horizontally and 100 m vertically. Relocated hypocenters were pinned to the absolute location determined for the M_L 2.1 event, preserving the relative locations.

Following the approach of Schaff and Richards (2014), the relative magnitudes of the earthquakes were estimated by comparing the unnormalized correlation coefficients of the events to the cataloged M_L 2.1 event. The estimation is given as

$$\delta\text{mag} = \log_{10}[\max(\mathbf{x}\bigstar\mathbf{y})/(\mathbf{x}\cdot\mathbf{x})],$$

in which ★ and · represent cross-correlation and dot product, **x** and **y** are the cataloged M_L 2.1 earthquake and a matched event, respectively. To validate these magnitude estimations, we also determined local magnitudes through a Richter scale approach similar to our previous work (e.g., Skoumal, Brudzinski, Currie, *et al.*, 2014). Although the two methods produced virtually identical magnitude estimations for the larger events, the Richter scale approach tended to overestimate the smaller magnitude events when poorer-quality stations were utilized. As demonstrated by Schaff and Richards (2014), correlation magnitude estimation techniques are ideally suited for estimating magnitudes of events with Gaussian white noise. Therefore, we utilized the correlation magnitude estimation in our analysis, which included the calculation of a Gutenberg–Richter *b*-value using the maximum-likelihood estimate (MLE).

To gain additional perspective on the stresses associated with this earthquake sequence, we calculated a fault-plane solution for the largest event, which was just large enough to make reliable identifications of first-motion polarities at local and nearby regional stations. Takeoff angles were estimated using the pseudobending method within *tomoDD* (Zhang and Thurber, 2003). We used *FocMec* to performed a grid search of the focal sphere for a double-couple solution (Snoke, 2003) and then took the median solution with zero polarity errors. A grid-search fit is justified by previous nearby studies that found clear double-couple mechanisms along apparently pre-existing basement faults (Kim, 2013; Skoumal *et al.*, 2015).

RESULTS

Using the three long-standing regional stations (M54A, N54A, and O56A), templates from the M_L 2.1 earthquake on 31 August identified the next two largest earthquakes, a 29 July 2014 M_L 1.5 and a 24 August 2014 M_L 0.1 event. Using the three closest TA stations (M53A, M54A, and N53A), three additional earthquakes with $M_L \sim 0$ were found around the timing of the two largest events. The six epicenters determined using

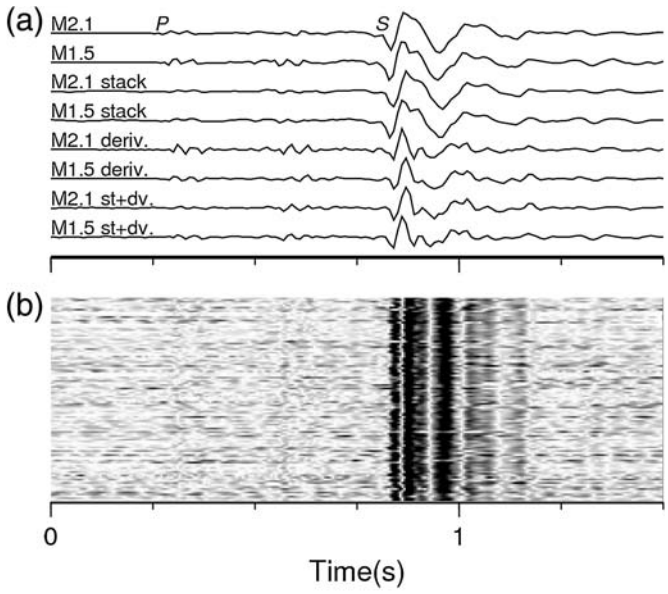

▲ **Figure 2.** Normalized *P* and *S* waveforms recorded on the BHE component of AWM4. (a) Template waveforms from the 31 August 2014 M_L 2.1 and 28 July 2014 M_L 1.5 earthquakes, as well as the stacks of events they matched with, derivatives of the template waveforms, and derivatives of the stacks. (b) Waveform amplitudes of the 108 matched events.

local data formed a band extending southwest of the well at distances 20–500 m from the wells in the basement at 3.1–3.3 km depth. Using the velocity model previously derived from nearby sonic logs (Kim, 2013), the absolute location errors for the M_L 2.1 were 60 m east–west and ~120 m north–south.

Utilizing local data, the multiple constructed templates identified 108 earthquakes with visually similar waveforms (Fig. 2): 70% of the events were detected using waveforms associated with the M_L 2.1 templates and 30% from the M_L 1.5 templates. Using the stack and derivative templates provided a 25% increase beyond just the original two event templates. The 102 additional events discovered using local data had M_L − 1.4 to 0, with a magnitude of completeness of approximately M_L − 1.0 based on the frequency–magnitude distribution (FMD).

The resulting set of all 108 matched events covers nearly the entire three-month period for which local data were obtained (Ⓔ Table S1), although there are only a handful of events during the first three weeks and after injection was halted (Fig. 3a). The low seismicity rates appear to extend before the time period of local data we analyzed, as we found no additional events when scanning single stations back to before injection began (P. Friberg, personal comm., 2015). The rate of very small ($M_L < 0$) seismic events tended to increase over time but appears to have done so episodically. The seismicity

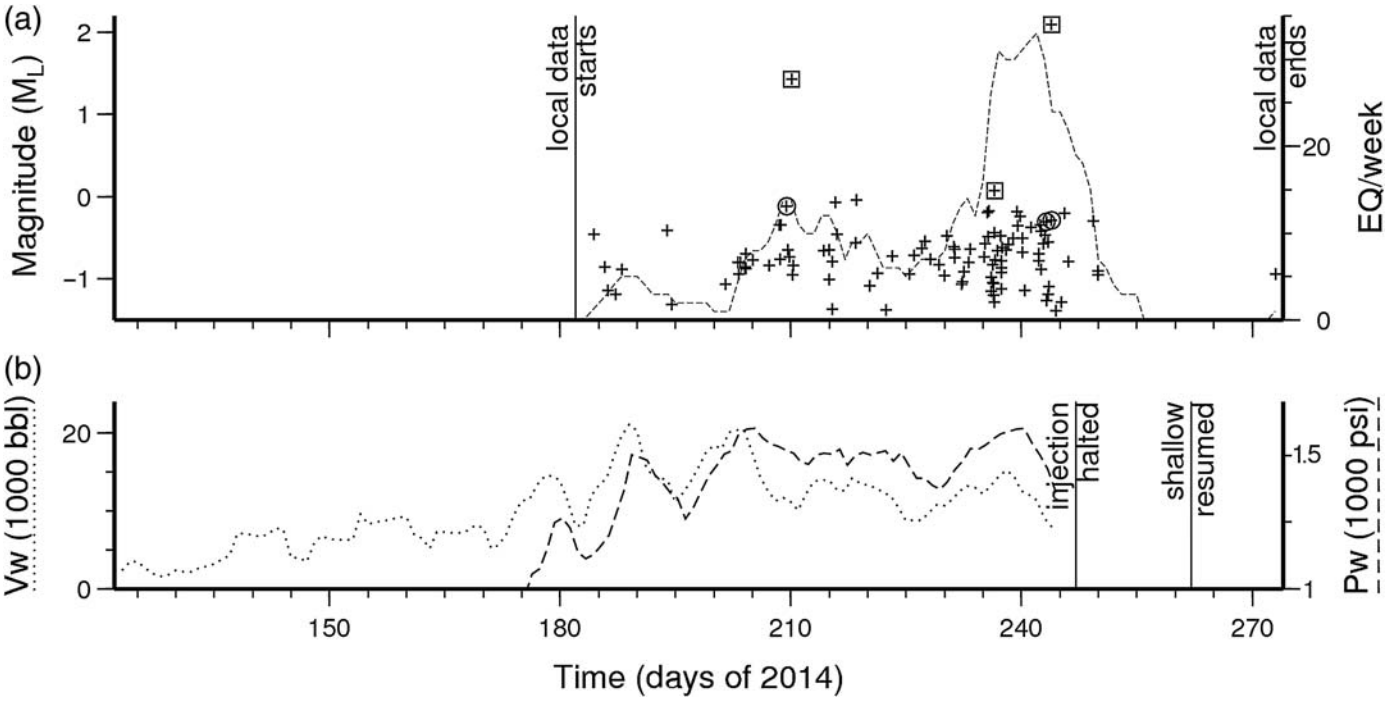

▲ **Figure 3.** (a) Magnitudes of matched events using cross correlation at the closest local station (crosses). The dashed line shows the rate of detected earthquakes per week. The vertical bars mark the time frame for which local data has been analyzed. The boxes containing plus symbols show events that were also detected by multiple combinations of regional stations (box) and events detected by the closest three regional stations (circle). No additional matches were found using regional data from November 2010 to January 2015. (b) Weekly averages of injection volume (V_w, dotted line) and pressure (P_w, dashed line). The vertical bars mark when the Ohio Department of Natural Resources (ODNR) ordered the injection halted and when injection was allowed to continue at American Water Management Services well 1 (AWMS-1).

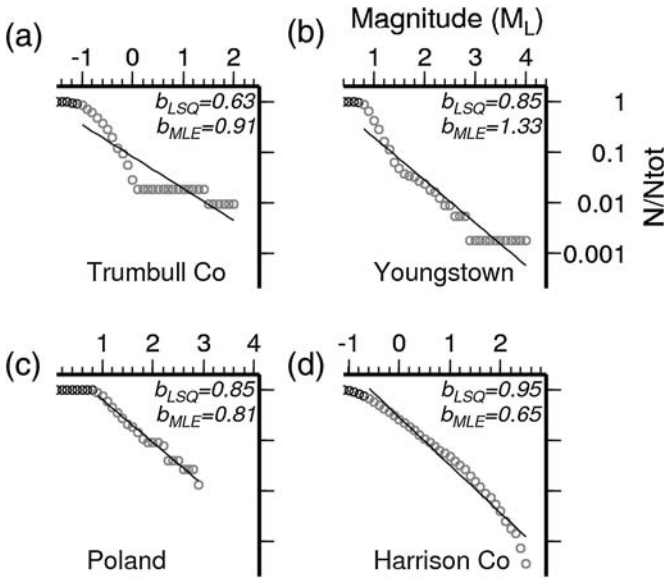

▲ **Figure 4.** Magnitude–frequency estimates (circles) comparing (a) this study to (b) another case of seismicity during wastewater injection near Youngstown (Skoumal, Brudzinski, Currie, *et al.*, 2014) and two cases of seismicity during hydraulic fracturing in (c) Poland Township (Skoumal *et al.*, 2015) and (d) Harrison County (Skoumal, Brudzinski, and Currie, 2014). The black circles are below the estimated M_c. *b*-values are for least-squares (LSQ, black line) power-law fit and maximum-likelihood estimate (MLE).

rate increased quickly in the week preceding both the M_L 1.5 and 2.1 event, followed by a significant rate decrease. The reduced rate after the larger events implies a low aftershock rate that is unexpected for a stable continental region (Ben-Zion and Lyakhovsky, 2006). The jump of more than an order of magnitude before the two larger events could be partly explained by the relatively narrow range of magnitudes in the remaineder of the events, such that the two larger events are anomalous.

The unusual pattern of earthquake magnitudes during this sequence is also evident in our attempts to estimate the Gutenberg–Richter *b*-value (Fig. 4). Although the *b*-value we calculate using the MLE method is close to 1 (0.91), the *b*-value we calculated using the least-squares (LSQ) method is 0.6. The discrepancy occurs because the FMD does not follow a power law and suggests a different relationship is at work. A similar trend can be observed at the Youngstown injection well, although with larger magnitude events. However, the other nearby earthquake sequences induced by hydraulic fracturing in Harrison County (Friberg *et al.*, 2014) and Poland Township (Skoumal *et al.*, 2015) appear to follow a more typical power-law FMD. In induced sequences with very high pore-fluid pressure, the viscosity of the fault zone could be dictated by the fluid, which would result in atypical FMDs. If fluid pressures are not as extreme, induced earthquakes may be followed by a sudden drop in pore pressure that could lead to more regular FMDs.

The earthquake activity appears to be correlated with injection at AWMS-2. The daily injection volumes provided to us by the AWMS are the total for both wells but are based on the totalizers; AWMS-2 took 95% of the total volume before activities were suspended (AWMS, personal comm., 2015). Figure 3b shows weekly averages for volume (V_w) and pressure (P_w) for AWMS-2. The earthquake rates appear to increase once sustained injection pressures approach the maximum allowed surface pressure of ~11.6 MPa (1680 psi). This corresponds to pressures at the base of the injection interval of ~39.5 MPa (~5727 psi) given an ~1.1 g/cm^3 maximum density of injected fluids and slight friction-related reduction in pressure due to flow in through the injection tubing at reported maximum rates of 2 barrels/ min (AWMS, personal comm., 2015).

It is also noteworthy that the volumes are reduced in late July once weekly pressures are near the maximum but the pressures only decrease slightly. When the volumes are raised again in late August, there is a corresponding increase in pressures and seismicity rate. After the injection was halted on 3 September, only three earthquakes were detected on 6 September. When the shallow injection was resumed on 18 September, we only found one earthquake on 30 September, about two days before the local data ends.

Figures 5 and 6 show map and cross-sectional views of the best located hypocenters with relative location bootstrap uncertainties <120 m horizontally and 150 m vertically. The average uncertainty of plotted events is ~60 m east–west, ~30 m north–south, and ~100 m vertically. The events form two clusters, one almost adjacent to the well and the other ~400 m southwest of the wells. The separation of these clusters was confirmed by performing absolute locations of the six largest events. The proximal cluster includes an event on 3 July, suggesting this cluster became active first, as one would expect for its proximity to the wells. The distal cluster became active on 13 July, but the M_L 1.5 event on 29 July occurred in the proximal cluster. Both clusters are active in August, but the M_L 2.1 event on 31 August occurred in the distal cluster. Intriguingly, the distal cluster has a north-northeast–south-southwest trend (024°) different from previous nearby cases, which followed an east-northeast–west-southwest trend (~080°). Although the trend in the proximal cluster is harder to estimate due to fewer events, it appears to have a more east-northeast–west-southwest trend that aligns with seismicity along the northern edge of the distal cluster. We note that seismicity in the distal cluster initiates during a drop in weekly averaged pressure (Fig. 3), which could indicate that fluid pressures migrating along a east-northeast–west-southwest fault drop upon reaching a north-northeast–south-southwest fault.

A sufficient number of *P*-wave first motions were available to calculate a focal mechanism for the M_L 2.1 event (Fig. 7). The fault-plane solution that we determined was a strike-slip mechanism, similar to previous nearby cases (Fig. 5), but it shows a different azimuthal trend. In this case, the east-southeast–west-northwest left-lateral fault-plane azimuth (110°) is rotated ~30° from the previous cases. This fault plane does not align well with either the overall trend of hypocenters or the trend of either event cluster. Instead, the north-northeast–south-southwest right-lateral fault-plane azimuth (020°) matches better

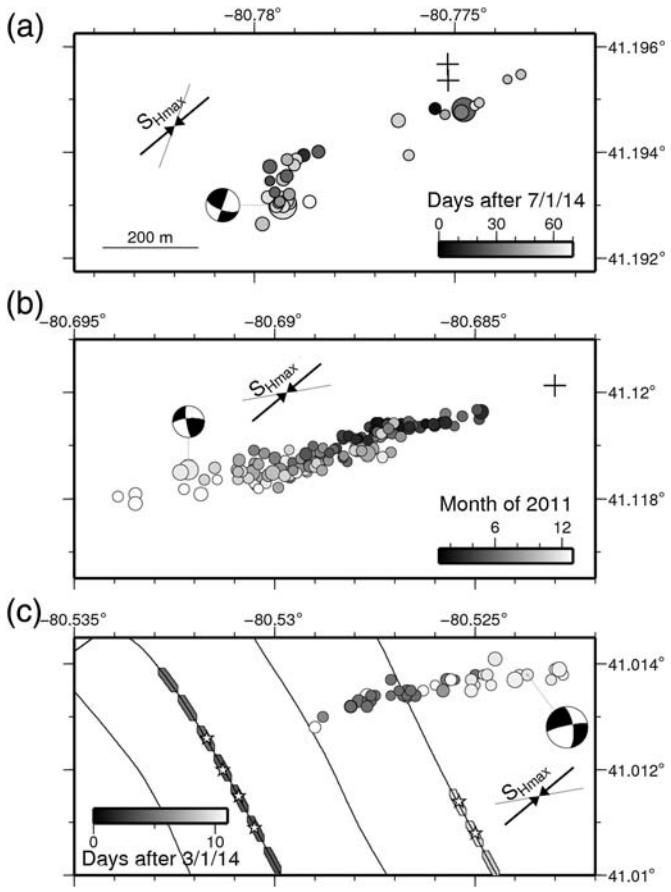

▲ **Figure 5.** Map of the double-difference relocated earthquakes for the (a) Trumbull, (b) Youngstown (Skoumal, Brudzinski, Currie, *et al.*, 2014), and (c) Poland Township, Ohio, (Skoumal *et al.*, 2015) sequences. Only the best-located events that exceeded a 12 × MAD NNCCC threshold are shown. The circles are scaled according to magnitude. Focal mechanisms are shown for the largest events in each sequence (this study; Kim, 2013; Skoumal *et al.*, 2015). The arrows show orientation of maximum horizontal stress, and the gray lines are the fault orientation suggested by focal mechanism and trend of hypocenters. In (a) and (b), the plus symbols represent the location of the injection wells. In (c), the black lines are the horizontal laterals of drilled wells, the ovals are completed fracture stages, and the stars denote stages temporally correlated with seismicity.

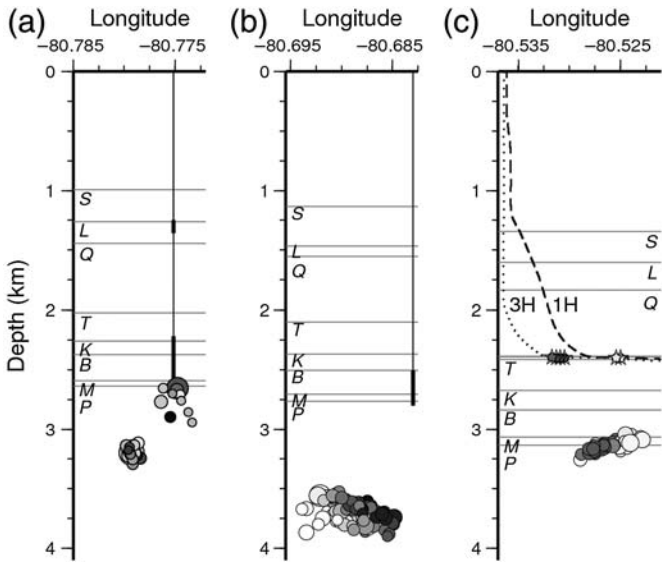

▲ **Figure 6.** East–west cross sections of the double-difference relocated seismicity for the (a) Trumbull, (b) Youngstown (Skoumal, Brudzinski, Currie, *et al.*, 2014), and (c) Poland Township, Ohio (Skoumal *et al.*, 2015). There is no vertical exaggeration. The horizontal gray lines mark key strata: S, Salina; L, Lockport; Q, Queenston; T, Trenton; K, Knox; B, B Zone; M, Mt Simon and P, Precambrian basement. In (a) and (b), the black vertical line represents the location of the injection well with the screened interval in bold. In (c), the dashed and dotted black lines represent the paths of two wells into the Point Pleasant (not labeled). The stars indicate fracture stages that were temporally correlated with seismicity. The shaded scales are the same as in Figure 5.

with the trend in the distal cluster in which the M_L 2.1 event occurred. To quantify this comparison, we investigated the distances of epicenters in the distal cluster from a fault plane with either orientation. The standard deviation of epicenters from a 020° fault plane is ~3 times less than the average relative location uncertainty in the east–west direction, whereas the standard deviation of epicenters from a 110° fault plane is ~2 times more than the average relative location uncertainty in the north–south direction.

The hypocentral depths we determined also indicate the events in the proximal cluster occurred near the top of the Precambrian crystalline basement in close proximity to the bottom of the deep well. The distal cluster of events is about 500 m deeper but still in the upper Precambrian. These two depth ranges are similar to the nearby Poland Township and Youngstown induced sequences (Fig. 6) (Skoumal, Brudzinski, Currie, *et al.*, 2014, 2015).

DISCUSSION

The likelihood of inducing slip along a pre-existing fault is greater if the injection well or hydraulic fracturing stimulation is near a critically stressed fault, that is, optimally oriented to the regional stress field. The focal mechanism and azimuthal trend of the distal cluster of seismicity in the Trumbull sequence outlined a potentially different fault orientation (~020°) than nearby induced sequences of Youngstown (078°; Skoumal, Brudzinski, Currie, *et al.*, 2014), Poland Township (083°; Skoumal *et al.*, 2015), and Harrison County (092°; Friberg *et al.*, 2014) (Fig. 1). However, the northeast–southwest orientations of the regional $S_{H\max}$ in eastern Ohio determined by Hurd and Zoback (2012) suggests that these two fault orientations (~020° and ~080°) are both ~30° from $S_{H\max}$ and hence are optimal orientations for reactivation. Although the proximal cluster of Trumbull seismicity is only a handful of events, it may represent an ~080° basement fault or fracture trend extending from the well toward the distal cluster. If so, all four Ohio cases would

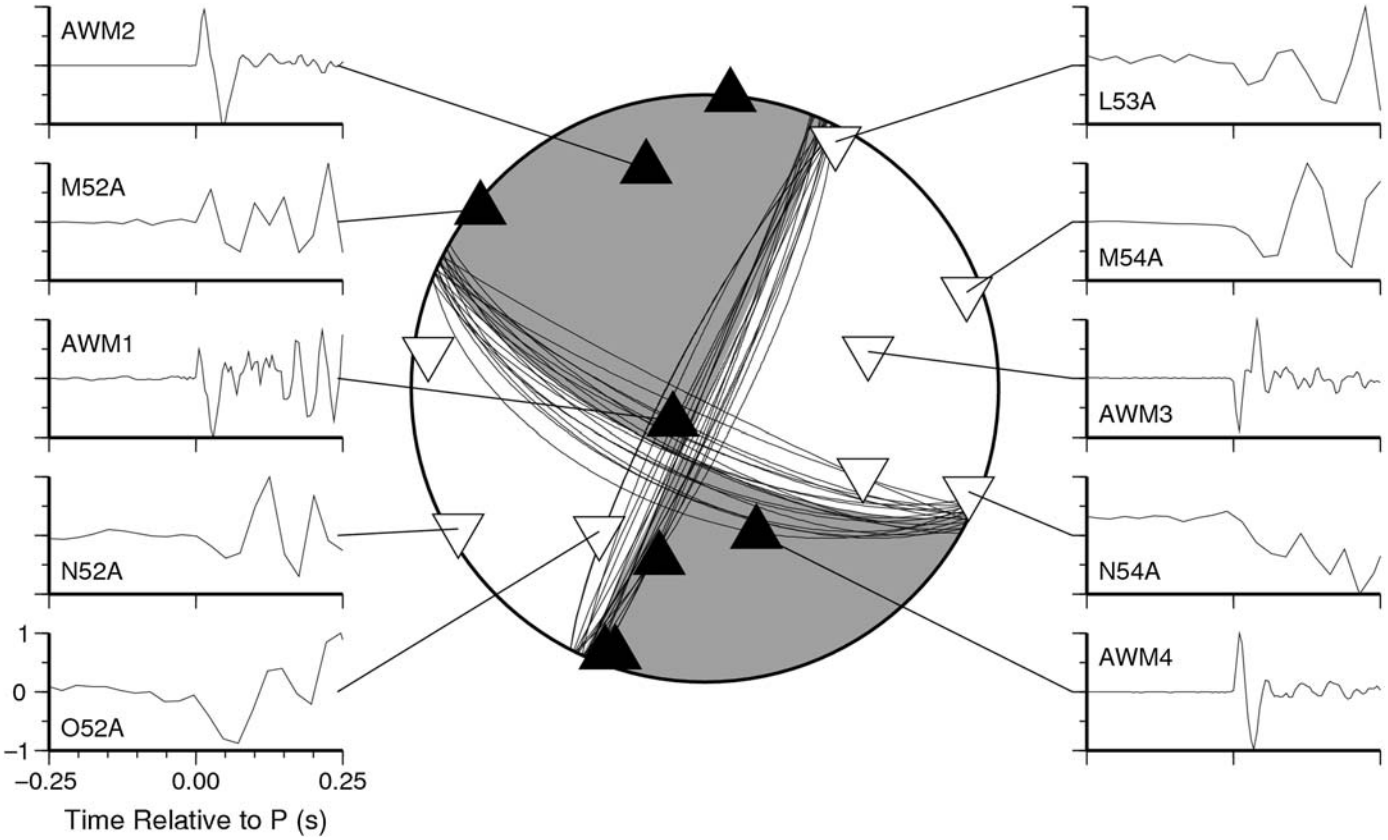

▲ **Figure 7.** Fault-plane solution and selected first arrival waveforms for the 31 August 2014 M_L 2.1 earthquake. Triangles on the focal sphere show station polarity data for compressional (black) and dilatational (white) first motions. Seismograms are filtered but not interpolated, showing 0.25 before and after the picked *P*-wave arrival time at each station.

represent ~500–800 m segments of strike-slip faults located within 1 km from the operations in map view. The slip appears to be located in the upper Precambrian basement in each case, such that there may be a network of faults or fractures in the shallow basement in eastern Ohio that are susceptible to being induced by human activities. A detailed study of the large number of injection wells and hydraulic fracturing stimulations that have not induced any detected seismicity could provide additional insight into the pervasiveness or scarcity of susceptible structures.

We recently proposed that induced earthquakes in Ohio could be identified using a checklist of possible indicators (Brudzinski *et al.*, 2014): a close spatial correlation (< 10 km) between anthropogenic activities and observed seismicity, a close temporal correlation (< 1–2 years) between activities and observed seismicity, a repetitive swarm of seismicity, a low *b*-value or nonpower-law FMD, and the seismicity occurs in a region with no previously documented earthquakes. All of these criteria appear to be met in the Trumbull case, but we can further determine whether both the shallow and deep wells (AMWS-1 and AMWS-2) are responsible. Once the injection operations at both the shallow and deep Trumbull wells were halted, the seismicity rate quickly decreased. Following the resumed operations of the shallow well (AWMS-1), we find a lack of small earthquakes ($M_L < 0$) in the weeks after using the local data and an absence of any larger earthquakes ($M_L > 0$) in the months after using the regional data. Combining this finding with the relatively small amount of water injected into AWMS-1 and the large spatial distance between AWMS-1 and the Precambrian basement, we do not believe AWMS-1 has influenced slip along the fault. It appears that the sequence is solely a result of injection into the deep well (AWMS-2).

When the conditions are suitable for inducing earthquakes, a number of studies have suggested the number and size of earthquakes are related to the volume of fluids injected (e.g., McGarr, 2014; Holtkamp *et al.*, 2015). This study supports those relationships in that the seismicity rate tends to increase with increasing cumulative injected volumes (Fig. 3). In fact, the increasing rate of very small ($M_L < 0$) seismicity was a potentially diagnostic feature that the sequence was induced. However, the decrease in injected volumes beginning in late July, while pressures remained relatively high, indicates the absence of a simple relationship between injected volumes and number of earthquakes. Figure 8 illustrates how the weekly seismicity rate correlates better with the weekly average well pressures than with the weekly average injected volumes. The trends are not linear, so we calculated a Spearman's rank correlation and found the correlation coefficient is 62% between pressure and earthquakes and −22% between volume and

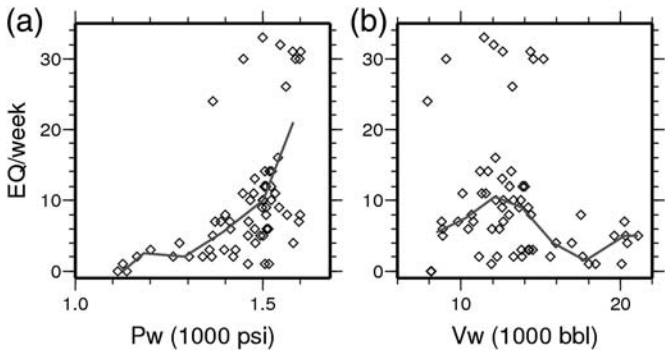

▲ **Figure 8.** Comparison between seismicity rates and average weekly (a) pressures and (b) volumes injected for each week during the local data availability. The trend lines are median values in eight evenly spaced bins.

earthquakes. The ~10% standard error indicates that correlation between pressure and earthquakes is much more statistically significant. The larger seismicity rates and majority of the earthquakes occur when the weekly average surface injection pressures are above 9.3 MPa (1350 psi). There appears to be a several-day lag between changes in well pressure and corresponding changes in seismicity rate (Fig. 3), which is similar to observations made in the Youngstown case (Holtkamp *et al.*, 2015) and implies a relatively fast communication between injection and seismic response.

Ellsworth (2013) identified two mechanisms for inducing earthquakes from wastewater injection: by (1) directly increasing the pore pressure along a fault or (2) changing the loading conditions above a fault. The pore-fluid pressure mechanism would require a high-permeability pathway between the well and the fault. The fluids are expected to migrate via diffusion and could progressively lower effective normal stress that promotes fault slip. The diffusion of the water would be expected to create a pore-pressure triggering front and back front when the high fluid pressure reaches and leaves the fault, respectively. Between the relatively slow-moving triggering fronts, shorter time-scale variations in fluid pressures could also induce fluid pressure waves that more rapidly transmit dynamic changes in pore-fluid pressure along the fault.

Inducing a fault to slip through loading conditions could be possible in wells that have injected large volumes of water above a fault over long time frames, like the Prague case in Oklahoma (Keranen *et al.*, 2013; Sumy *et al.*, 2014). In this mechanism, the fluid pressure waves would not have to reach the fault. Rather, the volume and/or mass change of injected fluids above a fault would alter the shear and normal stresses, promoting slip. For the Trumbull and Youngstown sequences, the close temporal correlation between injection operations and seismicity are indications that fluid pressure changes are changing the effective normal stresses directly on the fault. However, the Trumbull sequence highlights three new observations from a wastewater injection case that also appear to be related: lack of aftershock productivity, narrow magnitude range, and nonpower-law FMD. Each of these observations is predicted by numerical simulations of a seismogenic zone governed by a viscoelastic damage rheology when the viscosity in the fault zone is reduced (Ben-Zion and Lyakhovsky, 2006). Such a reduction in viscosity is expected if deep wastewater injection increases fluid pressures in the fault zone to the point that the fault zone begins to dilate.

The formation of new fractures from hydraulic fracturing is expected to produce microseismicity with $M_L < 1$ and a b-value of ~2 (Maxwell *et al.*, 2009; Wessels *et al.*, 2011; Warpinski *et al.*, 2012). Although rare, inducing a pre-existing fault to slip from hydraulic fracturing has been documented to produce seismicity with b-values < 1 and magnitudes up to M_L 4.2, as seen in the Septimus basin in British Columbia (e.g., British Columbia Oil and Gas Commission (BCOGC), 2014; Skoumal *et al.*, 2015). Two mechanisms are suggested for inducing earthquakes by hydraulic fracturing: (1) changes in viscoelastic stress transmitted primarily through rock and (2) changes in pore pressure transmitted through pore space. Tomographic imaging near wells undergoing hydraulic fracturing suggest pre-existing faults can be activated by viscoelastic stressing as much as 1 km horizontally and vertically from the borehole (Lacazette and Geiser, 2013). Those distances are harder to explain with fluid pressures considering the rapid onset and halt of seismicity with individual stages on the order of minutes in some cases. Moreover, the volumes injected and the duration of injection are both considerably smaller than for disposal wells. Using the Trumbull sequence as a guide, fluid pressure changes could result in lack of aftershock productivity, narrow magnitude range, and nonpower-law FMD; however, these patterns are generally absent in the Poland Township and Harrison County cases, so we propose those cases are due to viscoelastic stressing.

Regardless of the specific mechanism for inducing seismicity, a number of cases of seismicity induced by fluid injection have been examined to investigate whether adjusting operations can reduce the degree to which seismicity is induced (NAS, 2012). The NAS report suggests that seismicity can be reduced by lowering injection volumes and pressures. Considering the majority of seismicity occurred in our study region once weekly average pressures were above 9.3 MPa despite reductions in injected volumes, we suggest that keeping the sustained pressures below this level, perhaps via a lower maximum pressure, would be a key criterion for reducing seismicity if injection is resumed at the deep AMWS-2 well. We also hope this study demonstrates the utility of template matching for detection and evaluation of microseismicity ($M_L < 1$), which could then be used to adjust injection operations to help ensure seismicity remains below regulatory limits.

CONCLUSIONS

Multistation cross-correlation template matching is a valuable tool to monitor for induced seismicity, in addition to providing a more refined analysis of past seismic sequences. Utilizing both regional and local networks, 108 earthquakes were identified < 500 m from a pair of injection wells in southern Trumbull

County, Ohio, between 3 July and 30 September 2014. These events ranged in size from $M_L - 1.4$ to 2.1, but there is a remarkable separation between the two largest events and the rest, leading to anonpower-law FMD. We also observed swarm behavior with low aftershock productivity for a continental interior. Each of these observations is consistent with recent numerical simulations when the viscosity in the fault zone is reduced by fluid injection. We suggest these could be diagnostic features that seismicity is being induced by injected fluid changing the pore-fluid pressures in the fault zone. The seismicity outlined a fault located in the uppermost Precambrian basement with an overall east-northeast trend similar to the orientation of other nearby induced sequences. However, the focal mechanism of the largest event and trend of the events cluster further from the well follow a northeast-north orientation. Both fault orientations are optimally oriented within the regional stress field. The operations at both wells were suspended by the ODNR on 3 September 2014. The lack of earthquakes after injection resumed at the shallower well (AWMS-1) and lack of earthquakes near this well during earlier injection indicates this well was not related to the seismicity and supports ODNR's decision to resume injection operations at this well. The deeper well (AWMS-2) is very likely related to the earthquakes based on strong spatial and temporal correlations between injection and seismicity. Although seismicity rates generally grew with larger cumulative-injected volumes, weekly seismicity rates were better correlated with weekly average well pressures. Seismicity primarily occurred when sustained pressures at AWMS-2 approached the maximum allowed, suggesting future deep injection at reduced pressures is a strategy that could preserve the current low seismicity rate. However, we advocate employing a multistation cross-correlation template matching approach in real time to monitor whether activity of microseismicity ($M_L < 1$) remains at low levels.

ACKNOWLEDGMENTS

Seismic data were obtained from the Incorporated Research Institutions for Seismology Data Management Center (IRIS) (www.iris.edu; last accessed February 2015). Plots were made using Generic Mapping Tools v.4.2.1 (www.soest.hawaii.edu/gmt; last accessed February 2015). Geophysical log interpretation software used in this study was supplied by the LMKR University Grant Program. Support for this work was provided by National Science Foundation Grant EAR-0847688 (to M. B.) and the Ohio Department of Natural Resources (ODNR). The ODNR provided critical data and information for this study, and we specifically thank M. Angle, D. Blake, S. Dade, J. Fox, M. Hansen, and T. Serenko for their assistance. S. Kilper and American Water Management Services (AWMS) provided injection volumes, pressures, and background information related to their wells. This research also benefited from discussions with P. Friberg, M. Hasting, B. Rish, and Y. Ben-Zion. This study benefitted greatly from the local network installed by M. Hasting and disposal reports provided by AWMS. Three anonymous reviewers and Zhigang Peng provided constructive reviews that significantly improved the manuscript. Our analysis relied heavily on Miami University's High Performance Computing, and we thank J. Mueller for his assistance.

REFERENCES

Barrett, S. A., and G. C. Beroza (2014). An empirical approach to subspace detection, *Seismol. Res. Lett.* **85,** no. 3, 594–600, doi: 10.1785/0220130152.

Ben-Zion, Y., and V. Lyakhovsky (2006). Analysis of aftershocks in a lithospheric model with seismogenic zone governed by damage rheology, *Geophys. J. Int.* **165,** 197–210.

British Columbia Oil and Gas Commission (BCOGC) (2014). *Investigation of Observed Seismicity in the Montney Trend*, http://www.bcogc.ca/investigation-observed-seismicity-montney-trend (last accessed February 2015).

Brudzinski, M. R., R. J. Skoumal, and B. C. Currie (2014). Optimizing multi-station template matching to identify and characterize induced seismicity in Ohio, presented at *2014 Fall Meeting, AGU*, San Francisco, California, 15–19 December, Abstract S51A–4438.

Ellsworth, W. L. (2013). Injection-induced earthquakes, *Science* **341,** doi: 10.1126/science.1225942.

Evans, K. F., A. Zappone, T. Kraft, N. Deichmann, and F. Moia (2012). A survey of the induced seismic responses to fluid injection in geothermal and CO_2 reservoirs in Europe, *Geothermics* **41,** 30–54, doi: 10.1016/j.geothermics.2011.08.002.

Friberg, P. A., G. M. Besana-Ostman, and I. Dricker (2014). Characterization of an earthquake sequence triggered by hydraulic fracturing in Harrison County Ohio, *Seismol. Res. Lett.* **85,** doi: 10.1785/0220140127.

Healy, J. H., W. W. Rubey, and D. T. Griggs (1968). The Denver earthquakes, *Science* **161,** 1301–1310, doi: 10.1126/science.161.3848.1301.

Herrmann, R.-B. (2004). *Computer Programs in Seismology*, Version 3.30-GSAC, http://www.eas.slu.edu/eqc/eqc_cps/CPS/CPS330.html (last accessed February 2015).

Holtkamp, S., M. R. Brudzinski, and B. S. Currie (2015). Regional detection and monitoring of injection-induced seismicity: Application to the 2010–12 Youngstown, Ohio seismic sequence, *AAPG Bull.* doi: 10.1306/03311513194

Hurd, O., and M. D. Zoback (2012). Intraplate earthquakes, regional stress and fault mechanics in the Central and Eastern US and Southeastern Canada, *Tectonophysics* **581,** 182–192.

Keranen, K. M., H. M. Savage, G. A. Abers, and E. S. Cochran (2013). Potentially induced earthquakes in Oklahoma, USA: Links between wastewater injection and the 2011 M_w 5.7 earthquake sequence, *Geology* **41,** 699–702, doi: 10.1130/G34045.1.

Kim, W.-Y. (2013). Induced seismicity associated with fluid injection into a deep well in Youngstown, Ohio, *J. Geophys. Res.* **118,** 3506–3518, doi: 10.1002/jgrb.50247.

Lacazette, A., and P. Geiser (2013). Comment on Davies et al., 2012—Hydraulic fractures: How far can they go? *Mar. Petrol. Geol.* **43,** doi: 10.1016/j.marpetgeo.2012.12.008.

Maxwell, S. C., M. Jones, R. Parker, S. Miong, S. Leaney, D. Dorval, D. D'Amico, J. Logel, E. Anderson, and K. Hammermaster (2009). Fault activation during hydraulic fracturing, *SEG Technical Program Expanded Abstracts*, 1552–1556, doi: 10.1190/1.3255145.

McGarr, A. (2014). Maximum magnitude earthquakes induced by fluid injection, *J. Geophys. Res.* **119**, no. 2, doi: 10.1002/2013JB010597.

McGarr, A., D. Simpson, and L. Seeber (2002). Case histories of induced and triggered seismicity, in W. Lee, H. Kanamori, P. Jennings, and C. Kisslinger (Editors), *International Handbook of Earthquake and Engineering Seismology*, Vol. 40, Academic Press, London, United Kingdom, 647–664.

National Academy of Sciences (NAS) (2012). *Induced Seismicity Potential in Energy Technologies*, National Academies Press, Washington, D.C., 225 pp.

Nicholson, C., and R. L. Wesson (1990). Earthquake hazard associated with deep well injection: A report to the U.S. Environmental Protection Agency, *U.S. Geol. Surv. Bull. 1951*, http://pubs.usgs.gov/bul/1951/report.pdf (last accessed Februrary 2015).

Ohio Department of Natural Resources (ODNR) (2012). *Preliminary Report on the Northstar 1 Class II Injection Well and the Seismic Events in the Youngstown, Ohio, Area*, 23 pp., available at http://oilandgas.ohiodnr.gov/portals/oilgas/downloads/northstar/reports/northstar-preliminary_report.pdf (last accessed March 2014).

Ohio Department of Natural Resources (ODNR) (2014). *Ohio Announces Tougher Permit Conditions for Drilling Activities Near Faults and Areas of Seismic Activity*, http://ohiodnr.gov/news/post/ohio-announces-tougher-permit-conditions-for-drilling-activities-near-faults-and-areas-of-seismic-activity (last accessed December 2014).

Schaff, D. P., and P. G. Richards (2014). Improvements in magnitude precision, using the statistics of relative amplitudes measured by cross correlation, *Geophys. J. Int.* **197,** no. 1, 335–350, doi: 10.1093/gji/ggt433.

Skoumal, R. J., M. R. Brudzinski, and B. C. Currie (2014). Earthquakes induced by hydraulic fracturing in Poland Township, Ohio, *American Geophysical Union*, San Francisco, California, 15–19 December, Abstracts, S51A–4431.

Skoumal, R. J., M. R. Brudzinski, and B. C. Currie (2015). Earthquakes induced by hydraulic fracturing in Poland Township, Ohio, *Bull. Seismol. Soc. Am.* **105,** no. 1, doi: 10.1785/0120140168.

Skoumal, R. J., M. R. Brudzinski, B. C. Currie, and J. Levy (2014). Optimizing multi-station earthquake template matching through re-examination of the Youngstown, Ohio, sequence, *Earth Planet. Sci. Lett.* **405,** 274–280, doi: 10.1016/j.epsl.2014.08.033.

Snoke, J. A. (2003). *FOCMEC: FOCal MEChanism Determinations*, Package, http://www.geol.vt.edu/outreach/vtso/focmec/ (last accessed February 2015).

Sumy, D. F., E. S. Cochran, K. M. Keranen, M. Wei, and G. A. Abers (2014). Observations of static Coulomb stress triggering of the November 2011 M 5.7 Oklahoma earthquake sequence, *J. Geophys. Res.* **119,** 1904–1923.

Waldhauser, F. (2001). Hypodd: A computer program to compute double-difference earthquake locations, *U.S. Geol. Sur. Open-File Rept, 01-113*.

Waldhauser, F., and W. L. Ellsworth (2000). A double-difference earthquake location algorithm: Method and application to the northern Hayward fault, California, *Bull. Seismol. Soc. Am.* **90,** 1353–1368.

Warpinski, N. R., J. Du, and U. Zimmer (2012). Measurements of hydraulic fracture-induced seismicity in gas shales, in *SPE Hydraulic Fracture Technology Conference*, The Woodlands, Texas, 6–8 February 2012, Soc. Pet. Eng. Abstract 151597.

Wessels, S., M. Kratz, and A. De La Pena (2011). Identifying fault activation during hydraulic stimulation in the Barnett shale: Source mechanisms, b values, and energy release analyses of microseismicity, *SEG Technical Program Expanded Abstracts*, San Antonio, Texas, 18–23 September.

Zhang, H., and C. H. Thurber (2003). Double-difference tomography: The method and its application to the Hayward fault, California, *Bull. Seismol. Soc. Am.* **93,** no. 5, 1875–1889.

Robert J. Skoumal
Michael R. Brudzinski
Brian S. Currie
Department of Geology and Environmental Earth Science
Miami University
620 E. Spring Street
Oxford, Ohio 45056 U.S.A.
skoumarj@miamioh.edu
brudzimr@miamioh.edu
curriebs@miamioh.edu

Published Online 8 July 2015